Special Issue Article

Institution of MECHANICAL ENGINEERS

Journal of SPORTS ENGINEERING AND TECHNOLOGY

Proc IMechE Part P:
J Sports Engineering and Technology
1–11

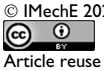
Article reuse guidelines:
sagepub.com/journals-permissions
DOI: 10.1177/1754337120912610
journals.sagepub.com/home/pip

Propulsive efficiency of alternative underwater flykick techniques for swimmers

Christopher WG Phillips, Alexander IJ Forrester, Dominic A Hudson and Stephen R Turnock

Abstract

Analysis of video and speed data is used to evaluate the efficiency of human underwater flykick. The authors show that by coupling Lighthill's theory of fish locomotion with human musculoskeletal modelling, it is possible to evaluate the effectiveness of the mechanical and hydrodynamic propulsive components of human underwater flykick. This allows the effect of subtle variances in technique to be assessed by measurement of athlete motion alone. This is demonstrated in an experimental case study of an elite athlete performing two different techniques; one more knee-based or thunniform, and the second more undulatory or carangiform/anguilliform. In finding the mean kinematics of each technique, it is first shown that maintaining stroke-by-stroke consistency of technique leads to an increase in propulsive efficiency. It is further demonstrated that in changing technique, an athlete may swim at the same kick rate but have different propulsive efficiency. This demonstrates the need to determine the energy cost in order to evaluate differing techniques. For the sprint athlete in this case study, it was shown to be more effective to swim with a thunniform technique when at higher velocities and a more anguilliform at lower velocities.

Keywords

Dolphin kick, underwater undulatory swimming, musculoskeletal model, propulsive efficiency, swimming

Date received: 21 May 2018; accepted: 21 January 2020

Introduction

Underwater flykick – often called underwater undulatory swimming (UUS), dolphin kick or the fifth stroke – is a form of human underwater swimming with techniques and strategies as varied as names. It is typically considered the fastest form of human swimming and consequently limited to 15 m per length in official swimming races. This constraint was first introduced in backstroke following the 1988 Olympic Games and subsequently in freestyle and butterfly following the the 1996 Olympic Games. In the 1988 men's 100 m backstroke heats, Berkoff set a new world record, swimming more than 30 m of the first leg underwater.[1] Later in 1996, Pankratov won the men's 100 m butterfly, having swum 40% of the race underwater.[2] Despite these demonstrations of effectiveness, athletes display a variety of techniques.[3] Many athletes in the London 2012 Olympic Games failed to take full advantage of the allocated distance.

It is typically opinion and intuition that are used to coach the swimmer, leading to differences in technique. For example, with regards to best technique, Von Loebbecke et al.[4] attribute most of the propulsive forces within the stroke to the region from just above the ankle to the toes and conclude that foot motion and ankle flexibility could have a large impact on performance. By contrast, Cohen et al.[5] suggest that ankle flexibility has little impact on net streamwise forces. It is therefore desirable to compare the effectiveness of variations in underwater flykick technique.

Drawing on experience of naval architecture, the aim of the work presented is to combine knowledge of hydrodynamic mechanisms, which convert specific human body motion into propulsion, with an inverse

Faculty of Engineering and the Environment, University of Southampton, Southampton, UK

Corresponding author:
Christopher Phillips, Faculty of Engineering and the Environment, University of Southampton, Room 3009, Building 176, Engineering Centre of Excellence, Boldrewood Innovation Campus, Southampton SO16 7QF, UK.
Email: chris.phillips@soton.ac.uk

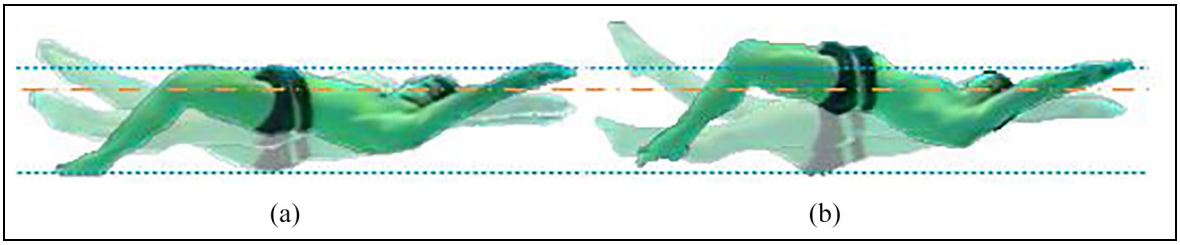

Figure 1. Comparison of body position at three instants through an underwater flykick. These correspond to maximum and minimum vertical range of toes as well as a near horizontal mid position. Images are centred on the head: (a) Technique 1 – thunniform, a more knee based kick and (b) Technique 2 – carangiform/anguilliform, whole body motion creates greater range of travel of feet.

analysis that infers the necessary human muscular activity required to generate such a motion. The achieved propulsive efficiency is thus deduced by relating useful output power to the actual muscular power required. This should also serve to narrow the gap between computation biomechanics and the actual human physiological energy expenditure, which Wei et al.[1] describe as remaining elusive.

Through indirect measurements, the authors demonstrate that the component stages of human underwater propulsive efficiency can be simulated using physics-based models. The influence of specific and often subtle changes in technique can then be understood through measurement of underwater motion alone, rather than by a more generalised equation based on kick frequency and forward velocity. A demonstration of this process is presented here in the form of a case study of a 50 m backstroke World Champion swimmer with two contrasting techniques of underwater flykick – one more thunniform (T_1) and the other more carangiform/anguilliform (T_2).

Ethical approval from the University of Southampton (FoHS-7207) and informed consent from the participant was sought prior to this study.

Flykick propulsive efficiency

The change in technique arises through a change in the athlete's kinematics, illustrated by the overlaid images in Figure 1. The images are aligned horizontally at the head for each technique, respectively, and vertically at the head between the two figures, as indicated by the dashed-dotted line. To compare the two, the maximum vertical displacement envelope of the hips in T_1 is outlined by the dotted lines across Figure 1. It can be observed how the displacement of the hips in T_2 exceeds this envelope in both the up and down phase of the kick cycle.

Anguilliform, carangiform and thunniform are terms used to describe fish kinematics,[6] with a decreasing amplitude of oscillation towards the head, respectively. The same terms have similarly been used to describe styles of human underwater swimming (e.g. Hochstein and Blickhan[7]). The first technique used here (T_1) can be seen to be a predominantly knee-based kick (Figure 1(a)) with only relatively small vertical displacement at the hips of the torso; akin to thunniform motion. The second technique (T_2), while still comprised of large knee range of motion, is more carangiform or anguilliform in so much as it exhibits a larger vertical displacement of the whole body, most apparent at the hips (Figure 1(b)).

The swimmer's motion occurs due to specifically timed muscle contractions, which develop a rearward wave-like motion that travels along the body. A propulsive thrust (body reaction) is produced, associated with the fluid momentum created. Consequently, the muscle contractions have to both move the limbs and work against the resistance to motion caused by the surrounding fluid. The swimmer's speed will be determined by the balance of thrust through the cycle against the resistance (or drag) of the body. The oscillatory motion of a swimmer's flykick can be characterised in terms of a Strouhal number (St) shown in equation (1) which relates how fast vortices are being generated (due to the oscillations of the feet) and the space between them.[8] In the context of human swimming this is often presented as

$$St = \frac{\bar{A}\bar{f}}{\bar{V}} \tag{1}$$

where $\bar{A}$ is the mean amplitude of the kick, $\bar{f}$ the mean kick frequency, and $\bar{V}$ the swimmer's mean velocity (e.g. Hochstein and Blickhan[7]). For example, a change in amplitude generates a change in the Strouhal number for a fixed frequency. This is analogous to the advance ratio (J) used for a ship propeller,[9] which relates translational speed to propeller rotation speed. A propeller's pitch is then modified to achieve maximum efficiency based on the conditions. Similarly, in flying animals, kinematics are tuned for an optimal St.[10,11] It is hypothesised that similar to altering the pitch of a propeller or kinematics of a wing, changing flykick technique will alter the Strouhal number to achieve a maximum efficiency. A comparison of typical Strouhal values for fish and cetaceans, human monofin swimming and underwater flykick is shown in Table 1. It demonstrates that typical Strouhal of underwater flykick are comparatively higher. The table also serves to illustrate the large range cited for Strouhal

Table 1. Published values of Strouhal numbers (*St*).

Description	*St*
Fish and cetaceans	0.2→0.4[12]
Human mono-fin	0.35→0.68[13]
Human underwater flykick	0.42→0.53[3]
	0.8→0.93[7]
	1.05→1.37[14]
	1.06→1.21[4]

number for human swimming which might reflect humans' sub-optimal technique in comparison to fish.

The powertrains of human swimming have been described by Daniel[15] and Zamparo et al.[16] Each stage of power transfer needs to be matched to the next in order to achieve a maximum overall efficiency, which typically for ships is expressed in terms of the ratio of effective power (P_E), the useful power to propel the ship, to power in ($\dot{E}$).[9] In the context of animal locomotion, however, this is referred to as drag efficiency (η_D), as shown in equation (2), such that

$$\eta_D = \frac{TV}{\dot{E}} \tag{2}$$

where T is the useful thrust, V the forward speed, and $\dot{E}$ the rate of energy supplied to the system.

Lighthill[17] and comparatively more recently Singh and Pedley[18] provide a theoretical approach to determining these forces for fish propulsion. Although there is potential to overestimate force magnitudes, it typically replicates the correct mean and trends[19,20] and is many orders of magnitude more rapid[21] than computational-based methods as covered by the review paper by Wei et al.,[1] with computational fluid dynamics (CFD) examples such as Von Loebbecke et al.[4] or smooth particle hydrodynamics of Cohen et al.[5]

Determining the relationship between muscular effort and propulsive thrust has been attempted for some swimming strokes using land-based machines. These measure the effective power delivered by an athlete and also their energy consumption by monitoring oxygen consumption (VO_2).[22] Alternatively, it is possible to simultaneously measure active drag[23–25] and metabolic power ($\dot{E}$) using VO_2 directly during swimming.[26] This enables athletes' aerobic energy expenditure and propulsion to be measured. Neither of these techniques are currently practical for underwater flykick.

Recent developments have seen the use of an inverse approach applied by a computational musculoskeletal model. This method infers the muscle forces necessary to develop a given kinematic motion and estimates each muscle's necessary length and activity.[27] Here, the muscle activity is defined as the force in each muscle normalised by the maximum force it can produce. Umberger[28] and Umberger et al.[29] found good agreement with experimental data when combining the energy of the mechanical element of the muscle with estimates for thermal energy liberation to evaluate total muscle energy expenditure. Langholz et al.[30] compared three musculoskeletal models to inform swimming analysis, finding the AnyBody modelling system[31] as the most sophisticated and favourable for investigations with focus on the interaction between the body and the environment. Earlier work in Japan coupled the SWUM model[32] with an AnyBody musculoskeletal model to investigate surface swimming,[33,34] finding sufficient agreement between experimental and simulated results. The AnyBody modelling system has also been used to develop the model in this study.

Using the fluid force and musculoskeletal data, the propulsive efficiency (η_P) of the underwater flykick technique is found by sub-dividing the drag efficiency of equation (2), into the efficiency stages where energy is lost, as shown in equation (3); metabolic efficiency (η_B, energy delivered to the muscles), muscle efficiency (η_M, energy delivered by the muscles), hydraulic efficiency (η_H, energy delivered to the fluid) and Froude efficiency (η_F, the proportion of useful energy deliver to fluid)

$$\eta_D = (\eta_B \cdot \eta_M) \cdot \eta_H \cdot \eta_F \tag{3}$$

The input chemical energy is converted into mechanical work out by the muscles (W_{tot}), the efficiencies for which are not assessed for this study. This work is then used to create the swimmer's motion, where the surface of the swimmer is opposed by the hydrostatic loading (buoyancy) and hydrodynamic motion of the surrounding fluid ($\int Qw + Tv\,dt$, where Q is the transverse force, T is the forward thrust, and w and v are the relative water velocity components). The final stage is the ratio of useful work ($\int Tv\,dt$) to that of the overall work done on the fluid. The total system can be expressed over an oscillatory cycle, as shown in equation (4)

$$\eta_D = (\eta_B \cdot \eta_M) \cdot \frac{\int Qw + Tv\,dt}{W_{tot}} \cdot \frac{\int Tv\,dt}{\int Qw + Tv\,dt} \tag{4}$$

The propulsive efficiency (the authors' metric of interest) is therefore the product of η_H and η_F and hence equation (5)

$$\eta_P = \frac{\int Tv\,dt}{W_{tot}} \tag{5}$$

Here, η_P for each technique is determined by the ratio between the useful work done (W_d) and the total mechanical work done by the muscles (W_{tot}), where W_d is shown in equation (6)

$$W_d = \int Tv\,dt \tag{6}$$

T is the calculated thrust, V is the measured speed of the athlete, and W_{tot} is shown in equation (7)

$$W_{tot} = \int F_i \cdot \dot{L}_i \, dt \tag{7}$$

where F_i is the force in the contractile element of the muscle, and $\dot{L}_i$ is the time derivative of the muscle length.

Experimental video and data capture is able to record the athlete's motion, as well as measure their speed.[35,36] Using these data as inputs, the remaining parameters in equations (6) and (7) can be estimated and hence η_P found.

Experimental case study

A world-class elite male backstroke specialist (height 1.82 m and mass 84 kg) performed the two techniques, T_1 and T_2, both in the supine position and within the same pool session. During both, he strived to maintain a constant depth and heading, and performed a minimum of 10 kicks for each technique. The first technique was his race-refined technique, thought to exhibit a more knee-based or thunniform style (T_1).

The second (T_2) strove towards a more anguilliform/carangiform technique, with a body wave originating from the shoulders, travelling through to the toes and growing in amplitude. The concept was that greater articulation of the pelvis would facilitate the growth of the generated wave along the body. After practising the new technique, the athlete repeated the acquisition process as before.

Synchronised image and speed data required for the study were acquired using a pool-based system.[13,21,36] As the body motion in underwater flykick is assumed symmetrical about the sagittal plane, two-dimensional kinematics were acquired from a submerged camera moving with the swimmer.

While the athlete performed the two techniques, their speed was measured by means of a trailing low-stretch, lightweight line and a rotary encoder. The line was connected to the athlete by a thin strap around their waist, in such a way as to not impinge on their motion. It was then wound around a reel connected to a rotary encoder, with a small resistance applied to prevent overspin. The rotary encoder converted the 250 pulses per revolution of the encoder into a linearly varying analogue voltage. This analogue source was calibrated and connected to a laptop via a 6009 NI™ USB analogue data acquisition board. The speed and video data were acquired and recorded at 250 and 25 Hz, respectively.

Kinematic processing

A MATLAB[37] script was used to analyse the kinematics of the 10 leg kicks by digitising the acquired video for the corresponding run. The joint centres and anatomical locations were selected in each frame. These are comprised of the tip of the toes, ankle, knee, hip, shoulder, wrist and fingertip. The elbow location is selected in the first frame and assumed to maintain a constant relative location between the shoulder and wrist throughout a run. Two consistent points are also selected on the upper and lower pelvis to provide its orientation (see Figure 2). The beginning of the up-kick signified the start of each cycle. The first phase of the cycle is, therefore, the extension of the knee joint and upwards movement of the toes until full extension is achieved. The second phase is the recovery of the legs initiated with knee flexion. The athlete's joint angles are defined using the joint coordinate system of the International Society of Biomechanics (ISB)[38] and used by AnyBody.

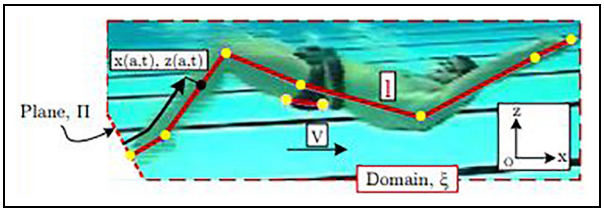

Figure 2. Lighthill reference system. Points indicate the digitised locations from which the joint angles are derived.

To explore the characteristic kinematics of T_1 and T_2, they were each subdivided into the 10 kick cycles. Each cycle was then normalised in time, and the characteristic mean joint angles and speed profile were obtained for the two conditions. A five-term Fourier series was subsequently fitted to these joint angle data. Using these coefficients, a further two data sets of 10 uniform kick cycles, $\bar{T}_1$ and $\bar{T}_2$, were created as synthesised kinematics based on the original T_1 and T_2, respectively.

To gain greater insight into the concept of tuning the kinematics around the synthesised $\bar{T}_1$ and $\bar{T}_2$, the Fourier amplitude coefficients had a scale factor k applied. A range of scale factors between 0.1 and 2 were applied in increments of 0.1. For values of $k < 1$, this reduces the amplitude of all the joint angles and conversely, increasing the amplitude of each joint angle when $k > 1$. Permutations of the synthesised base kinematics for technique one and two, were then labelled $\bar{T}_{1\cdot k}$ and $\bar{T}_{2\cdot k}$ respectively, where k is indicative of the applied scaling factor.

Hydrodynamic forces: Lighthill's theory

Lighthill[17] analysed the thrust generation of fish using a momentum conservation approach. Numerically, this can be achieved by sectioning a fish or swimmer into n equal strips along its length, where each strip may be described in global coordinates in terms of a parametric distance a along the body at time t, as given schematically in Figure 2. Lighthill defines a bound area ξ, encapsulating the fish's motion, but excluding the wake, and hence is bound by plane Π at the fish's tail, which remains perpendicular to the tip. The rate of change of momentum in this control volume has terms

of (a) the rate of change due to convection of momentum out of ξ across plane Π; (b) plus the rate of change due to pressure forces acting across Π; and (c) minus the reactive forces with which the fluid acts on the fish.

For the prescribed kinematics, the thrust generated for propelling the fish through the water (T) and the transverse force acting on the fish (Q) is expressed as shown in equation (8)

$$(T, Q) = \left[mw\left(\frac{\partial z}{\partial t}, -\frac{\partial x}{\partial t}\right) - \left(\frac{1}{2}mw^2\frac{\partial x}{\partial a}, -\frac{\partial z}{\partial a}\right)\right]_{a=0} - \frac{d}{dt}\int_0^l mw\left(-\frac{\partial z}{\partial a}, \frac{\partial x}{\partial a}\right)da \quad (8)$$

where m is the mass per unit length ($m(a) = 0.25\pi\rho s(a)^2$, where ρ is the water density and s is the depth of the cross-section) and w is the velocity component perpendicular to the direction of parameter a. The depth of the cross-section along the body (s) was obtained from a commercial three-dimensional scan of the athlete. The widths were measured at the feet, ankle, knee, upper-thigh, upper-arm, elbow wrist and hand. Assuming symmetry in the sagittal plane, these values were doubled and appended to the list containing the width of the torso at the naval and shoulders and the neck. The widths $s(a)$ were, therefore, estimated by linearly interpreting the measure points with respect to distance s along the body.

For T_1 and T_2, experimental speed data were used. However, for $\bar{T}_{1\cdot k}$ and $\bar{T}_{2\cdot k}$, a mean speed was used as an initial input to the Lighthill model. This speed was determined based on the original experimental data. For the two techniques, an equivalent mean drag coefficient (C_D) was determined using equation (9)

$$\bar{T} = \frac{1}{2}\rho\bar{V}^2SC_D \quad (9)$$

where $\bar{T}$ is the mean thrust, ρ is the density of the water, $\bar{V}$ is the athlete's mean speed, and S is the frontal area (assumed proportional to kick amplitude (A) $\times$ breadth at pelvis (B)).

Using the initial mean speed for the respective technique, the Lighthill simulation was executed to calculate the mean thrust, and based on the previously calculated drag coefficient, a new mean speed was estimated. This process was iterated until the mean speed converged ($< 0.003\ \mathrm{ms}^{-1}$, typically by the third iteration). The resulting transverse forces (Q) were then used as inputs for the musculoskeletal simulation in the form of body segment loads.

Musculoskeletal model

Figure 6 shows the musculoskeletal model scaled to the height and mass of the athlete. As the influence of the arm motion would be small, these were excluded. Table 2 details the number of simulated muscles in groups and other kinematic components divided between the body segments.

Table 2. Audit of the musculoskeletal model.

Description	Quantity
Rigid body segments	36
Rigid body DOFs	222
Frictionless joints	137
Explicit/implicit drivers	85
Muscles in trunk	203
Muscles in each leg	158
Total muscles	519

DOF: degree of freedom.

In order to deduce the muscle activities, AnyBody employs an inverse dynamics solver for which the kinematics and external forces must be defined. In this study, the driven kinematics were: the z-axis of rotation for the pelvis segment relative to the global origin; ankle-plantar, knee and hip flexion; and pelvis-thorax extension. The model had over-determined kinematics since there are more muscles than degrees of freedom. The AnyBody default third-order polynomial recruitment solver[39] was used to estimate the normalised muscle activity of each muscle (x_i, where $i \in \{1, \ldots, M\}$ where M is the total number of muscles). For any motion generated by the body, it is supposed that it will be achieved in the most efficient way across all the muscles, minimising the necessary energy and delaying fatigue.[40] AnyBody provides the simple metric of maximum muscle activity, which here has been used as a surrogate for efficiency when comparing the techniques.

The muscles were collated into groups associated with specific joint motions for later analysis. These included the flexors and extensors of the pelvis-thorax, hip, knee and ankle and core muscles.

Results and discussion

The Lighthill and musculoskeletal simulations took approximately 30 min to solve for each technique (10 kicks per technique on a 64-bit Win7 (SP1) PC, Intel quad-core 2.67 GHz processor and 12 GB RAM) with the key results shown in Table 3. It shows that an 11.2% reduction in mean maximum muscle activity ($\bar{M}_{max}$) was observed for T_2 compared to T_1. Similarly, there was a reduction in mean muscle activity in the trunk ($\bar{A}_{T}r$) and the legs ($\bar{A}_{LL} + \bar{A}_{RL}$), with the legs experiencing the highest reduction (26.2%) and consequently a relative shift in muscle loadings ($\bar{A}_{L:T}$) of 8.8% from the legs to torso.

Despite a 12.4% calculated reduction in thrust, the measured speed was only reduced by $0.04\ \mathrm{ms}^{-1}$ (with no significant difference found for either parameter). This implies that the total resistance of the athlete in the second trial must also have been reduced.

For each technique, there are two peaks of positive thrust. Figure 3(a) shows the maximum coinciding with

Table 3. Results from the simulations for T_1 and T_2.

	T_1	SD	T_2	SD	$T_1 \rightarrow T_2$ (%)	p value
$\bar{M}_{max}$	0.84	(0.60)	0.75	(0.55)	−11.2	0.056
$\bar{A}_{tot}$	11.92	(4.75)	9.18	(3.82)	−23.0	*
$\bar{A}_{Tr}$	5.33	(2.42)	4.31	(2.12)	−19.1	*
$\bar{A}_{LL}$	3.30	(1.63)	2.43	(1.23)	−26.2	*
$\bar{A}_{L:T}$	1.24	((0.13)	1.13	(0.05)	−8.8	*
$\bar{T}$(N)	99.1	(353)	86.8	(492)	−12.4	ns
$\bar{V}$(ms^{-1})	1.90	(0.13)	1.86	(0.15)	−2.2	ns
W_{tot} (Nm)	3981	(45.0)	4223	(32.0)	6.1	*
W_d (Nm)	693	(175)	729	(185)	5.2	ns
η_P	0.174		0.173		−0.8	0.011
St	0.96	(0.05)	1.0	(0.06)	0.3	ns
$\bar{f}$(Hz)	2.75	(0.09)	2.23	(0.09)	−18.8	*
$\bar{A}$ (m)	0.66	(0.03)	0.8	(0.04)	20.0	*

Mean maximum muscle activity ($\bar{M}_{max}$), mean total activity ($\bar{A}_{tot}$), mean trunk activity ($\bar{A}_{Tr}$), mean left leg activity ($\bar{A}_{LL}$), ratio of mean left leg to trunk activity ($\bar{A}_{L:T}$), mean thrust ($\bar{T}$), mean velocity ($\bar{V}$), total muscle work ($\bar{W}_{tot}$), useful work out ($\bar{W}_d$), propulsive efficiency (η_P), mean Strouhal number (St), mean kick frequency ($\bar{f}$) and mean kick amplitude ($\bar{A}$).
*$p < 0.01$.

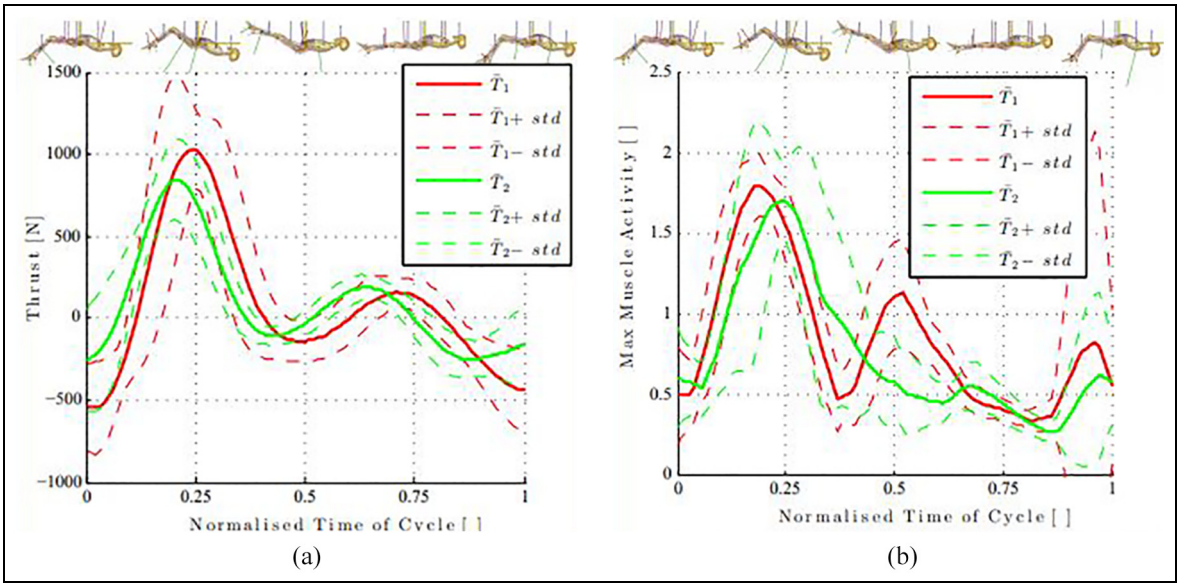

Figure 3. Normalised to one cycle: (a) shows the mean thrust for $\bar{T}_1$ (red or dark) and $\bar{T}_2$ (green or light) and (b) the mean muscle activity for $\bar{T}_1$ (red or dark) and $\bar{T}_2$ (green or light). The dashed lines and the dotted lines are one standard deviation above and below the relative data: (a) thrust and (b) maximum muscle activity.

change of direction of the toes as the knee and hip joints begin to extend. This implies that the extension phase of the kick produces significantly more thrust than the flexion phase.[5,41]

It was found that for T_1 and T_2, respectively, 95.5% and 92.3% of the net thrust originated from the foot segment, in agreement with Von Loebbecke et al.[4] It is also observed that combined, the shank and foot segments produce 95.1% of the total net thrust for T_1, a reduction from the foot segment alone.

From Figure 3(a), it can be seen that the peak of the mean thrust (standard deviation) from the 10 cycles was 841(247) N and 1031(275) N for T_1 and T_2, respectively. The male athlete in the study by Von Loebbecke et al.[4] produced a peak thrust of approximately 750 N; however, this was recorded at a mean velocity of 1.31 ms^{-1}, compared to 1.86 ms^{-1} in T_2. This variation could be attributed to the participating athlete in this study being a good sprint athlete and considered to be good at underwater flykick, or the combination of the velocity disparity. This could also be attributed to the kinematic variation, which is shown to produce inter-cycle variation in thrust and velocity (see Figure 3).

It is interesting to note that the Strouhal number has remained relatively unchanged, despite the changes in $\bar{f}$ and $\bar{A}$. This may illustrate a natural response to the body's power limit, or an element of subconscious maintenance of perceived efficiency by the athlete.

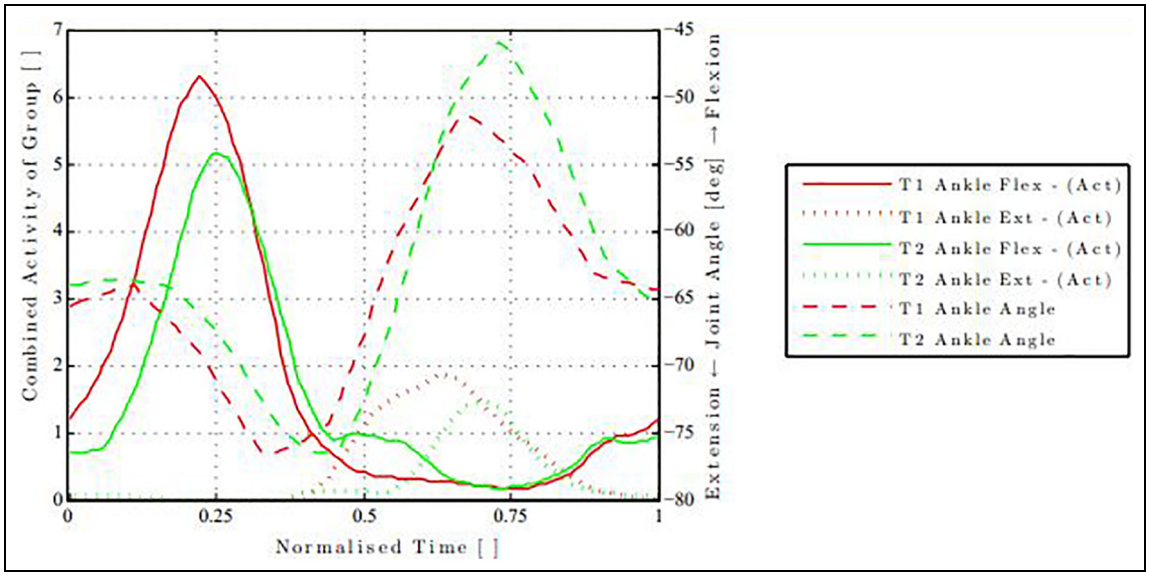

Figure 4. Flexor (solid) and extensor (short dash) activity of the ankle joint for T_1 (red or dark) and T_2 (green or light), with the context of ankle flexion angle (long dash).

Furthermore, with the maintenance of Strouhal number, the muscle activities between runs may be directly compared.

The maximum muscle activity for these simulations can be seen to peak at roughly the same phase of the cycle as the peak thrust (Figure 3) as the knee begins to extend. There is also a smaller secondary peak in the maximum muscle activity for the first technique, which is not present in the second (Figure 3(b)). This occurs as the toes change direction from the extension phase to the flexion phase and the knee begins to flex. Upon inspection of Figure 3(a) and (b), it is apparent that the cycle is divided into a thrust, followed by a recovery phase. The first half of the cycle (the extension phase) generated 86.2% and 83.2% ($\bar{T}_1$ and $\bar{T}_2$, respectively) of total propulsive thrust and 64.9% and 70.7% of total muscle activity ($\bar{T}_1$ and $\bar{T}_2$).

Using the musculoskeletal model, it is possible to investigate in more depth which muscles and muscle groups are being recruited at which part of the cycle and to what level of activity.

Figure 4 presents an example of the activity pattern of the combined muscles for the ankle joint. It shows the maximum activity of the grouped muscles coinciding with the maximum rate of joint angle motion. It also highlights the variation in motion between $\bar{T}_1$ and $\bar{T}_2$. For example, it can be seen that there is a reduction in peak activity for both the ankle flexor and extensor groups. There is a phasing difference, particularly prevalent in the second period of the cycle; the joint angle in $\bar{T}_2$ reduces more for a lower peak in the extensors' activity.

The activity for each of the combined muscles is shown in groups in Figure 5. An increase in combined activity can be observed in the core stabiliser muscles throughout T_2 as compared to T_1. With many of the stabilising muscles found in the trunk, it can also be seen in the apparent shift of muscle activity from the legs to the trunk (–8.8%, see Table 3). There is also a change in activity pattern for the pelvis-thorax extensors. This is most apparent at ~0.7 of the cycle, where there is an increase in activity which is less prevalent in $\bar{T}_1$.

There is a difference between the phasing of the activations between the trials. There are two distinguishable peaks visible in the two cases, but for $\bar{T}_1$ the first and second occur at ~0.19 and ~0.49 of the cycle, compared with ~0.25 and ~0.7 for $\bar{T}_2$.

This process of analysis also allows for inspection of individual muscles, as well as groups. Upon inspection of the individual muscle group data, it is found that Rectus Abdominis ($i = 195$, see Figure 6) and Biceps Femoris Caput Longum ($i = 67$, see Figure 6) in the trunk and legs, respectively, contribute greatly to the activity required to produce the motion for both techniques. They each exceed activity levels of 0.75 for the longest duration of any of the muscles in their respective areas of the body, and hence, this is indicative of their significance in underwater flykick. Rectus abdominis is associated with pelvic–thoracic flexion and biceps femoris caput longum with posterior extension of the hip joint, while forming part of the hamstring group for knee flexion in conjunction with caput brevis. It is envisaged that information of this kind could be beneficial in the holistic training and development of the specific athlete.

Umberger[28] used a complex musculoskeletal model to quantify the energy cost of locomotion (C_s) for a gait cycle. Here, a simplified mechanical model was used to estimate the energy expenditure for the two techniques using equation (7). This amounted to $C_s = 0.569$ and 0.502 $\mathrm{kJm^{-1}}$ for T_1 and T_2, respectively. These values,

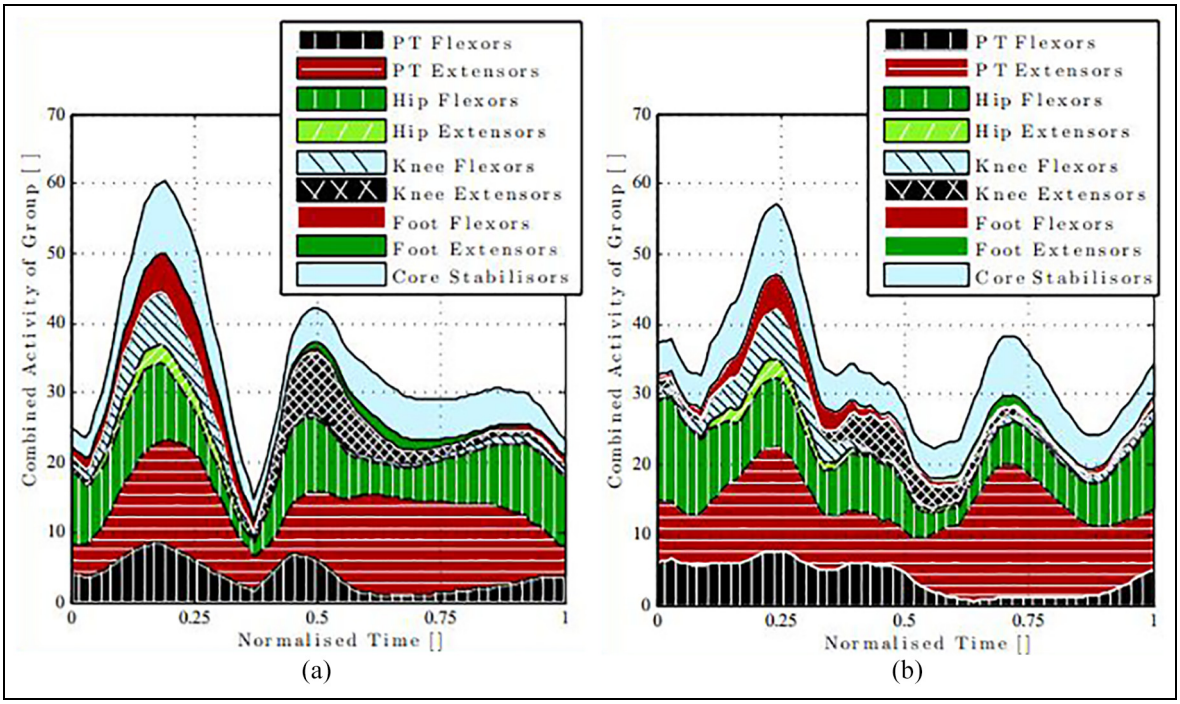

Figure 5. Area plot of combined activity of each muscle separated into the respective activity group: (a) $\bar{T}_1$ and (b) $\bar{T}_2$.

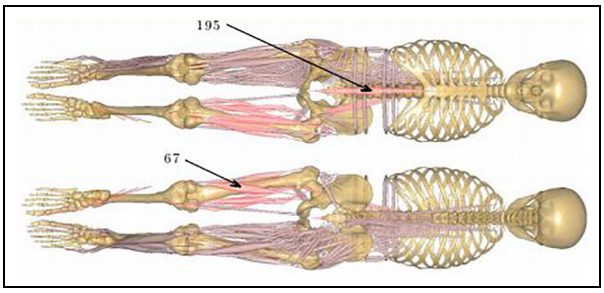

Figure 6. Coronal plane of the musculoskeletal model in anterior and posterior views. Showing all muscles on the body's right while those muscles on body's left are indicative of those with a higher frequency of activation. Those highlighted on the left have activity levels that exceed 0.75 for more than 5% of the cycle. Indicated muscles 195 and 67 are rectus abdominis and biceps femoris caput longum, respectively.

however, are low in comparison to experimental values for freestyle; albeit a less-efficient stroke. This could be attributed to: the actual variation in kinematics between the stokes; reduction in drag due to diminished interaction with free surface effects; the exclusion of the arms in the simulation; a simplified model for estimating energy expenditure based on mechanical work of the muscles which excludes the metabolic and muscle efficiencies and hence does not account for energy of thermal liberation as by Umberger et al.[29]

Nevertheless, this approach produces an approximation of the energy expenditure of human underwater swimming that is derived from the kinematics of a specific technique and is of particular benefit in comparative studies as demonstrated here.

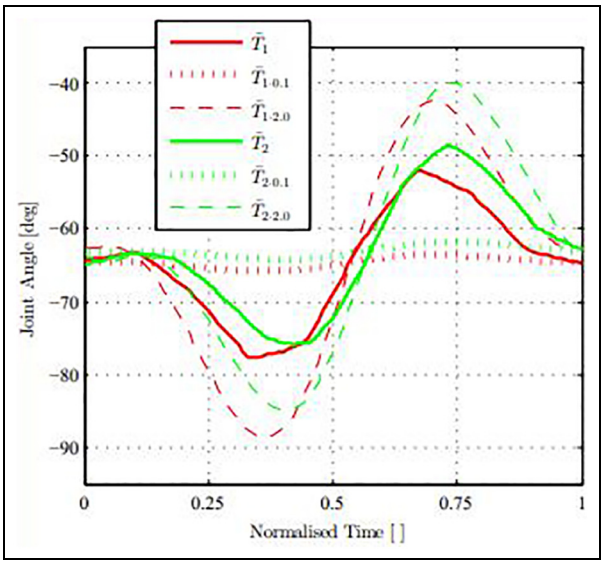

Figure 7. Example joint angle data obtained for ankle joint. The solid dark and light lines are the experimental data from $\bar{T}_1$ and $\bar{T}_2$, respectively. The short dashed lines are the minimum and long dashed lines the maximum from the data sets $\bar{T}_{1\cdot k}$ and $\bar{T}_{2\cdot k}$.

Tuning kinematics

The data sets $\bar{T}_{1\cdot k}$ and $\bar{T}_{2\cdot k}$ can provide insight into the tuning of the kinematics for the two techniques simulated here. Figure 7 shows the range of these joint angles with the example of the ankle angle. The solid lines are equivalent to the characteristic joint angles for $\bar{T}_1$ and $\bar{T}_2$ with the short and short dashed lines showing the extremes $k = 0.1$ and $k = 2$ respectively.

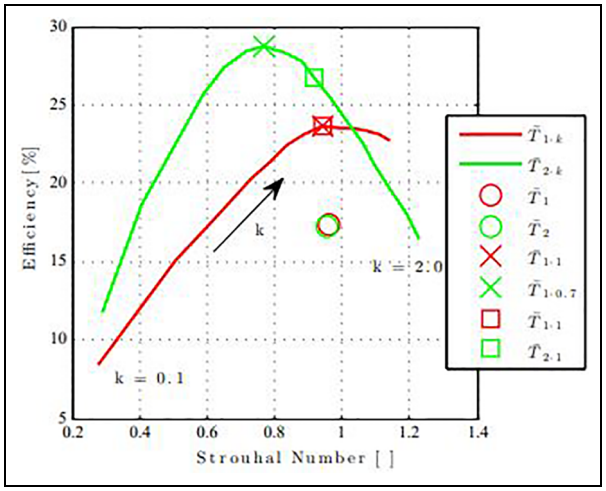

Figure 8. Relationship between kick amplitude and efficiency. The 'o' identify the mean Strouhal number and efficiency for $\bar{T}_1$ and $\bar{T}_2$. Dark and light solid lines represent $\bar{T}_{1\cdot k}$ and $\bar{T}_{2\cdot k}$ respectively. The '□' indicates when $k = 1$ and the '×' indicates peak efficiency, which for $\bar{T}_{1\cdot k}$ is at $k = 1.0$ and $\bar{T}_{2\cdot k}$ at $k = 0.7$. Maximum η_P for $\bar{T}_{1\cdot k}$ and $\bar{T}_{2\cdot k}$ occurs at $St_1 = 0.94$ and $St_2 = 0.77$, respectively.

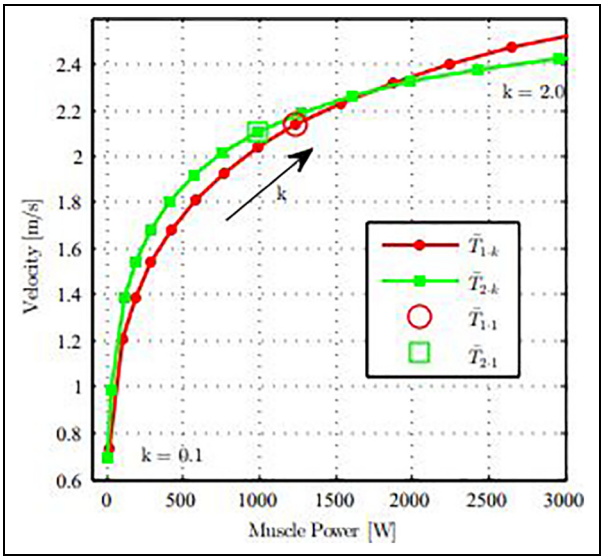

Figure 9. Relationship between power delivered by the muscles and swimming velocities for a sweep of k with $\bar{T}_{1\cdot k}$ and $\bar{T}_{2\cdot k}$ red or dark and green or light lines, respectively.

The propulsive efficiencies for a sweep of k are shown in Figure 8 as a function of Strouhal number, illustrating the non-linear relationship between the kinematic variations in $\bar{T}_{1\cdot k}$ and $\bar{T}_{2\cdot k}$.

It is apparent that there is an increase in efficiency from T_1 (red or dark circle) to $\bar{T}_{1\cdot 1}$ (red or dark square) and similarly from T_2 (green or light circle) to $\bar{T}_{2\cdot 1}$ (green or light square). The cause of this difference is attributed to the inter-cycle variation in T_1 and T_2 of which there are none in the characteristic data sets $\bar{T}_1$ and $\bar{T}_2$. This increase suggests that the maintenance of consistent kinematics generates higher observed efficiency.

The data indicate that the base style ($k = 1$) for the first technique (red or dark square) is at the optimal efficiency point for that technique (red or dark cross). Contrastingly, the base style for the second technique (green or light square) is not at the optimal efficiency point (green or light cross) – a decrease in the global joint angles would increase the efficiency of this technique to a maximum. This further illustrates the non-linear relationship between Strouhal number and η_P and clearly demonstrates the principle that tuning kinematics, as shown for flying animals,[11] can achieve higher efficiency in underwater flykick. In changing technique, this study has demonstrated that this athlete may swim at the same Strouhal number, but at a different value of propulsive efficiency.

The Strouhal numbers for $\bar{T}_1$ and $\bar{T}_2$ were 0.96 and 1.0, respectively, but with peak efficiency between 0.77 and 0.96 for the synthesised kinematics. It is interesting to note that fish and cetaceans are shown to have an optimal range of Strouhal numbers between 0.25 and 0.4.[8] However, in human underwater flykick, as seen in Figure 3(a), there appears to be only one significant thrust production and hence one vortex shed during the cycle (Figure 11 of von Loebbecke et al.[4]). This is in contrast to fish swimming and human mono-fin swimming, which have two.[7,13]

If it is considered that the frequency component in equation (1) is correctly defined as the frequency between vortex shedding, then the apparent time period between the generated vortices for underwater flykick is double that of mono-fin and fish swimming, and thus relatively half the frequency. This would therefore lead to a two-fold overestimation of Strouhal number for cases where only one vortex is shed in a cycle, such as demonstrated for underwater flykick. This would account for the large variation in theoretically optimal ranges in the published values of Strouhal number for human underwater flykick, relative to mono-fin and fish swimming.

Depending on a particular strategy, maximising efficiency may occasionally be misleading. For example, for T_1, it may be hypothetically less efficient to choose to swim at a lower Strouhal number. However, with an inverse relationship between velocity and Strouhal number, it may well be faster. This also illustrates the necessity to be able to determine the energy cost as simply the Strouhal number may be misleading.

From examining these results, it may be more effective for this sprint athlete to swim at a higher velocity and hence aim for a lower Strouhal number. Figure 9 displays the muscle power versus velocity for a sweep of k values, for both $\bar{T}_{1\cdot k}$ and $\bar{T}_{2\cdot k}$, where muscle power is simply the muscle work done (equation (7)) divided by time. Upon observation of Figure 9, for example, it may be more effective for the sprint athlete in this study to select a more knee-based kick of the first technique ($\bar{T}_1$) when swimming above 2.3 ms^{-1}. The reciprocal would therefore be more appropriate for lower velocities or for a longer distance swimmer, where

conservation of energy is more applicable. It may also be beneficial to shift from $\bar{T}_1$ to $\bar{T}_2$ as the athlete slows down following a start or push off the wall in a turn.

Conclusion

Lighthill's theory of fish locomotion has been coupled with a musculoskeletal model for the analysis of underwater flykick, allowing different underwater flykick techniques to be compared. An athlete's speed and kinematics were acquired and synchronised using a setup that is neither motion restrictive, nor invasive. Initial observations suggest the thrust production of Lighthill is comparable to published data; however, further and more detailed analysis should be conducted to validate and quantify this. In comparison to other methods, Lighthill is computationally inexpensive. The musculoskeletal model has been shown to provide significant insight into inter- and intra-simulated techniques, for example, highlighting the potential for an increase in efficiency associated with a consistent technique. The musculoskeletal model also facilitated the estimation of energetic cost of locomotion. The process was also able to identify muscles or muscle groups of significance that were associated with the simulated kinematics. It is considered that such information could be helpful in designing training or rehabilitation programmes.

An example of varying joint amplitude has demonstrated the potential benefit of tuning kinematics to provide a potential increase in efficiency. This provides a quantitative answer as to which technique may be preferable for this individual athlete when competing in short swimming events. It is suggested that initially following a dive, it would be preferable for this athlete to begin with a knee-based technique and transition to a more undulatory technique as their velocity decreases.

Declaration of conflicting interests

The author(s) declared no potential conflicts of interest with respect to the research, authorship, and/or publication of this article.

Funding

The author(s) disclosed receipt of the following financial support for the research, authorship, and/or publication of this article: This research was supported by the EPSRC (grant reference EP/H501568/1).

ORCID iD

Christopher WG Phillips https://orcid.org/0000-0002-6315-474X

References

1. Wei T, Mark R and Hutchison S. The fluid dynamics of competitive swimming. *Annu Rev Fluid Mech* 2014; 46(1): 547–565.
2. Forman S. Swimming at the 1996 Atlanta Summer Games: men's 200 metres Butterfly, 1996, http://www.sports-reference.com/olympics/summer/1996/SWI/mens-200-metres-butterfly.html
3. Collard L, Auvray E and Bellaunay I. Comparison of performance levels over 25 m by 11 expert swimmers using anguilliform-like and carangiform-like techniques: eel-like swimming versus carangiform-like swimming. *Int J Perf Anal Spor* 2011; 11(1): 26–33.
4. Von Loebbecke A, Mittal R, Mark R, et al. A computational method for analysis of underwater dolphin kick hydrodynamics in human swimming. *Sport Biomech* 2009; 8(1): 60–77.
5. Cohen RC, Cleary PW and Mason BR. Simulations of dolphin kick swimming using smoothed particle hydrodynamics. *Hum Movement Sci* 2012; 31(3): 604–619.
6. Vogel S. *Life in moving fluids: The physical biology of flow*. Princeton, NJ: Princeton University Press, 1994.
7. Hochstein S and Blickhan R. Vortex re-capturing and kinematics in human underwater undulatory swimming. *Hum Movement Sci* 2011; 30(5): 998–1007.
8. Rohr J and Fish FE. Strouhal numbers and optimization of swimming by odontocete cetaceans. *J Exp Biol* 2004; 207(10): 1633–1642.
9. Molland AF, Turnock SR and Hudson DA. *Ship resistance and propulsion: Practical estimation of ship propulsive power*. 1st ed. New York: Cambridge University Press, 2011.
10. Nudds RL, Taylor GK and Thomas ALR. Tuning of Strouhal number for high propulsive efficiency accurately predicts how wingbeat frequency and stroke amplitude relate and scale with size and flight speed in birds. *P Roy Soc B: Biol Sci* 2004; 271(1552): 2071–2076.
11. Taylor GK, Nudds RL and Thomas ALR. Flying and swimming animals cruise at a Strouhal number tuned for high power efficiency. *Nature* 2003; 425(6959): 707–711.
12. Triantafyllou G, Triantafyllou M and Grosenbaugh M. Optimal thrust development in oscillating foils with application to fish propulsion. *J Fluid Struct* 1993; 7(2): 205–224.
13. Nicolas G, Bideau B, Colobert B, et al. How are Strouhal number, drag, and efficiency adjusted in high level underwater monofin-swimming? *Hum Movement Sci* 2007; 26(3): 426–442.
14. Von Loebbecke A, Mittal R, Fish FE, et al. Propulsive efficiency of the underwater dolphin kick in humans. *J Biomech Eng* 2009; 131(5): 054504.
15. Daniel T. Efficiency in aquatic locomotion: limitations from single cells to animals. In: Blake RW (ed.) *Efficiency and economy in animal physiology* (Cambridge environmental chemistry series). Cambridge: Cambridge University Press, 2005, pp.83–95.
16. Zamparo P, Pendergast DR, Termin B, et al. How fins affect the economy and efficiency of human swimming. *J Exp Biol* 2002; 205(Pt 17): 2665–2676.
17. Lighthill MJ. Large-amplitude elongated-body theory of fish locomotion. *P Roy Soc B: Biol Sci* 1971; 179(1055): 125–138.
18. Singh K and Pedley T. Modelling lateral manoeuvres in fish. *J Fluid Mech* 2012; 697: 1–34.
19. Bertetto AM, Picasso B and Ruggiu M. Fish and ships: can fish inspired propulsion outperform traditional propulsion based systems? *Built Environ* 2001; 53: 279–287.

20. Borazjani I and Sotiropoulos F. Numerical investigation of the hydrodynamics of carangiform swimming in the transitional and inertial flow regimes. *J Exp Biol* 2008; 211(Pt 10): 1541–1558.
21. Webb AP, Phillips CW, Hudson DA, et al. Can Lighthill's elongated body theory predict hydrodynamic forces in underwater undulatory swimming? *Procedia Engineer* 2012; 34: 724–729.
22. Zamparo P and Swaine IL. Mechanical and propelling efficiency in swimming derived from exercise using a laboratory-based whole-body swimming ergometer. *J Appl Physiol* 2012; 113(4): 584–594.
23. Hollander A, de Groot G, van Ingen Schenau G, et al. Measurement of active drag during crawl arm stroke swimming. *J Sport Sci* 1986; 4(1): 21–30.
24. Kolmogorov S and Duplishcheva O. Active drag, useful mechanical power output and hydrodynamic force coefficient in different swimming strokes at maximal velocity. *J Biomech* 1992; 25(3): 311–318.
25. Webb AP, Banks J, Phillips CW, et al. Prediction of passive and active drag in swimming. *Procedia Engineer* 2011; 13: 133–140.
26. Reis VM, Marinho DA, Barbosa FP, et al. Examining the accumulated oxygen deficit method in breaststroke swimming. *Eur J Appl Physiol* 2010; 109(6): 1129–1135.
27. Damsgaard M, Rasmussen J, Christensen ST, et al. Analysis of musculoskeletal systems in the AnyBody modeling system. *Simul Model Pract Th* 2006; 14(8): 1100–1111.
28. Umberger BR. Stance and swing phase costs in human walking. *J R Soc Interface* 2010; 7(50): 1329–1340.
29. Umberger BR, Gerritsen KG and Martin PE. A model of human muscle energy expenditure. *Comput Method Biomec* 2003; 6(2): 99–111.
30. Langholz JB, Westman G and Karlsteen M. Musculoskeletal modelling in sports – evaluation of different software tools with focus on swimming. *Procedia Engineer* 2016; 147: 281–287.
31. AnyBody™ Technology. The AnyBody™ modeling system, 2011, http://www.anybodytech.com/fileadmin/AnyBody/Docs/Tutorials/main/main.html
32. Nakashima M, Satou K and Miura Y. Development of swimming human simulation model considering rigid body dynamics and unsteady fluid force for whole body. *J Fluid Sci Technol* 2007; 2(1): 56–67.
33. Nakashima M and Yugo M. Development of a full-body musculo-skeletal simulator for swimming. In: *11th international symposium on computer simulation in biomechanics*, 2007, pp.59–60, http://www.swum.org/Nakashima&Motegi(2007)Development%20of%20a%20full-body%20musculoskeletal%20simulator%20for%20swimming.pdf
34. Nakashima M, Hasegawa T, Kamiya S, et al. Musculoskeletal simulation of the breaststroke. *J Biomech Sci Eng* 2013; 8(2): 152–163.
35. Webb AP, Turnock SR, Hudson DA, et al. Repeatable techniques for assessing changes in passive swimming resistance. *J Biomech* 2013; 229(2): 126–135.
36. Phillips CW, Forrester AI, Hudson Da, et al. Comparison of kinematic acquisition methods for musculoskeletal analysis of underwater flykick. *Procedia Engineer* 2014; 72: 56–61.
37. The MathWorks Inc. MATLAB. Natick, MA: The MathWorks Inc, 2012.
38. Wu G, Siegler S, Allard P, et al. ISB recommendation on definitions of joint coordinate system of various joints for the reporting of human joint motion – part I: ankle, hip, and spine. *J Biomech* 2002; 35(4): 543–548.
39. AnyBody™ Technology. The AnyBody™ managed model repository, 2013, http://www.anybodytech.com
40. Rasmussen J, Damsgaard M and Voigt M. Muscle recruitment by the min/max criterion – a comparative numerical study. *J Biomech* 2001; 34(3): 409–415.
41. Von Loebbecke A, Mittal R, Fish FE, et al. A comparison of the kinematics of the dolphin kick in humans and cetaceans. *Hum Movement Sci* 2009; 28(1): 99–112.